

Supplementary Information

Title: Computational design of ligand binding membrane receptors with high selectivity

Authors: Feng, X.¹, Ambia, J.^{1,#}, Chen, K-Y.^{2,#}, Young, M.² & Barth, P.^{1,2,3,¶}

¶ Correspondences should be addressed to: P.B. (patrickb@bcm.edu)

¹ Department of Pharmacology, Baylor College of Medicine, One Baylor Plaza, Houston, TX 77030, USA.

² Verna and Marrs McLean Department of Biochemistry and Molecular Biology, Baylor College of Medicine, One Baylor Plaza, Houston, TX 77030, USA.

³ Structural and Computational Biology and Molecular Biophysics Graduate Program, Baylor College of Medicine, One Baylor Plaza, Houston, TX 77030, USA.

† Present address: Center for Petroleum and Geosystems Engineering, Cockrell School of Engineering, The University of Texas at Austin, Austin, TX 78712, USA

§ Present address: Department of Cell Biology and Human Anatomy, University of California at Davis, 4303 Tupper Hall, Davis, CA 95616, USA.

Supplementary Results

Supplementary Tables

Supplementary Table 1. Structural accuracy of ligand binding pose prediction.

Sequence identity between target and template GPCRs over full length and ligand binding region. Comparison between 3 homology modeling and ligand docking methods: classic Rosetta “sequential”; combination of Modeller and Glide, new “integrated” IPHoLD for 2 metrics: Ligand heavy atom rmsd (Lrmsd) and Native ligand-receptor atomic contact recovery (Method). Sequence identity between target and template is reported for the entire aligned receptor sequence and for the ligand binding region which includes the extracellular half of the TM region and part of the extracellular loop 2 (Method). *: For CRF1R, the ligand binding region is defined by the intracellular half of transmembrane helices 3, 5 and 6 that form the binding pocket for the ligand.

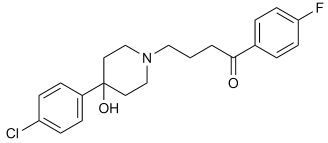
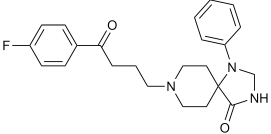
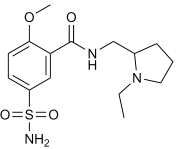
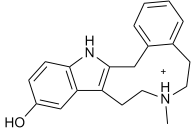
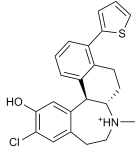
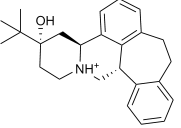
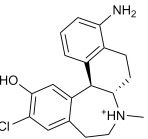
Target	Template	Sequence identity on full length (%)	Sequence identity on binding region (%)	Lrmsd (Å)			Native atom contact recovery (%)		
				Rosetta	Modeller /Glide	IPHoLD	Rosetta	Modeller/ Glide	IPHoLD
B2AR (2RH1)	DRD3 (3PBL)	34.0	28.0	9.4	9.7	1.4	22.7	22.7	96.0
B2AR (3D4S)	H1R (3RZE)	30.9	34.6	3.1	1.5	1.6	50.0	73.6	72.1
B1AR (2VT4)	H1R (3RZE)	30.8	27.8	2.9	3.1	1.6	54.1	61.0	72.1
H1R (3RZE)	M2R (3UON)	36.5	29.8	5.0	5.0	1.1	18.8	37.7	62.4
M2R (3UON)	H1R (3RZE)	34.3	28.1	3.5	13.0	1.0	40.3	0.0	79.1
DRD3 (3PBL)	B2AR (2RH1)	33.0	28.0	3.5	7.5	2.1	53.2	19.4	71.0
KOR (4DJH)	H1R (3RZE)	26.4	28.4	6.1	6.4	2.1	10.2	25.0	43.2
CCR5 (4MBS)	CXCR4 (3ODU)	31.5	34.4	5.1	8.2	2.1	22.1	16.3	51.2
5HT1B (4IAR)	DRD3 (3PBL)	37.4	35.6	3.4	4.4	1.4	46.7	44.4	58.9
5HT2B (4IB4)	DRD3 (3PBL)	33.0	29.4	3.6	7.3	1.9	32.7	15.8	52.6
CXCR4 (3ODU)	CCR5 (4MBS)	31.3	34.4	5.4	5.1	4.0	12.2	28.6	16.3
A2aR (3EML)	B1AR (2VT4)	33.0	24.5	5.7	4.8	3.9	32.0	32.0	33.3
SPH1 (3V2W)	B1AR (2VT4)	23.6	23.1	5.3	4.3	2.2	32.0	20.6	41.3
OPRL1 (4EA3)	DRD3 (3PBL)	25.3	25.5	4.9	9.1	3.3	18.4	3.3	66.7
A2aR (3UZA)	B1AR (2VT4)	33.0	24.5	6.1	7.0	2.0	17.2	19.0	67.2
δ-OR (4N6H)	AT1R (4ZUD)	31.3	25.0	5.6	7.1	2.8	19.4	19.4	34.3
AT1R (4YAY)	CCR5 (4MBS)	30.6	34.3	3.2	1.5	2.0	51.9	78.5	69.6
M3R (4DAJ)	H1R (3RZE)	29.7	33.3	3.2	5.5	1.4	55.2	22.4	70.1
OX1R (4ZJ8)	DRD3 (3PBL)	25.9	20.4	4.4	6.5	2.8	11.2	1.4	42.3
FFAR1 (4PHU)	PAR1 (3VW7)	20.4	23.2	7.8	8.2	2.6	18.5	7.6	53.3
CRF1R (4K5Y)	GCGR (5EE7)	33.7	42.1*	9.0	9.5	2.2	3.3	0.0	76.7
B2AR (2RH1)	B1AR (2VT4)	63.1	68.5	1.2	0.7	1.1	90.7	98.7	98.7
Average:				4.9	6.2	2.1	32.4	29.4	60.4

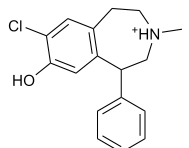
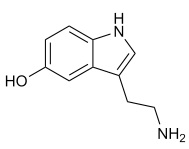
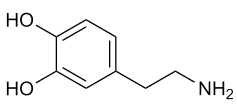
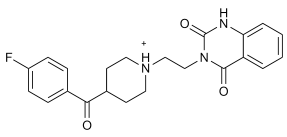
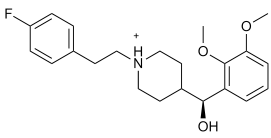
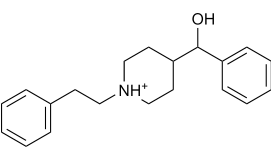
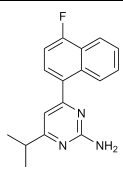
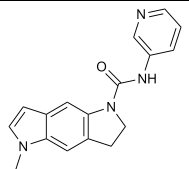
Supplementary Table 2. Structural accuracy of ligand binding site prediction.

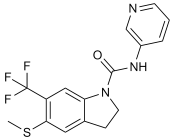
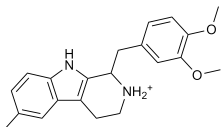
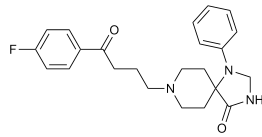
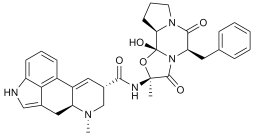
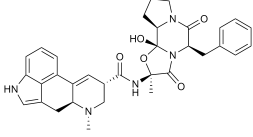
Comparison between 3 homology modeling and ligand docking methods: Rosetta; Modeller/Glide; IPHoLD for 2 rmsd metrics: over “ligand binding region” (extracellular half of TMHs and extracellular loop 2) and over residues in direct interaction with the ligand (i.e. with at least one heavy atom within 4 Å of a ligand atom, “interacting residues”). For CRF1R, the ligand binding region is defined by the intracellular half of transmembrane helices 3, 5 and 6 that form the binding pocket for the ligand.

Target	Template	Ligand binding region Ca RMSD (Å)			Interacting residues Ca RMSD (Å)			Interacting residues heavy atom RMSD (Å)		
		Rosetta	Modeller/ Glide	IPHoLD	Rosetta	Modeller/ Glide	IPHoLD	Rosetta	Modeller/ Glide	IPHoLD
B2AR (2RH1)	DRD3 (3PBL)	1.7	1.5	1.7	2.1	1.2	1.5	2.7	2.3	2.2
B2AR (3D4S)	H1R (3RZE)	1.6	2.0	1.6	1.4	1.8	1.7	2.8	2.5	2.9
B1AR (2VT4)	H1R (3RZE)	1.8	1.3	1.7	2.5	3.2	2.5	3.0	4.1	3.1
H1R (3RZE)	M2R (3UON)	1.6	1.2	1.3	1.2	0.9	0.9	3.3	2.6	2.2
M2R (3UON)	H1R (3RZE)	2.2	1.2	1.8	1.6	0.9	1.3	2.8	2.6	3.0
DRD3 (3PBL)	B2AR (2RH1)	1.5	1.2	1.3	1.4	1.0	1.0	1.9	1.8	1.7
KOR (4DJH)	H1R (3RZE)	2.6	3.2	2.5	3.0	2.5	1.4	4.0	3.5	2.7
CCR5 (4MBS)	CXCR (3ODU)	2.0	2.0	2.0	1.6	1.6	1.6	2.3	2.4	2.5
5HT1B (4IAR)	DRD3 (3PBL)	1.8	1.5	1.5	2.0	1.2	1.5	2.6	2.5	2.4
5HT2B (4IB4)	DRD3 (3PBL)	1.5	1.4	1.2	1.9	1.4	1.1	2.8	2.5	2.2
CXCR4 (3ODU)	CCR5 (4MBS)	2.4	1.9	1.9	0.9	0.7	1.2	2.3	2.4	2.3
A2aR (3EML)	B1AR (2VT4)	2.1	2.1	2.4	3.2	2.7	2.4	3.8	3.2	3.0
SPH1 (3V2W)	B1AR (2VT4)	1.8	2.1	1.6	2.9	3.6	2.5	4.1	4.5	3.5
OPRL1 (4EA3)	DRD3 (3PBL)	2.5	3.0	2.1	2.3	1.3	1.7	3.6	2.4	2.5
A2aR (3UZA)	B1AR (2VT4)	2.1	2.1	1.4	2.8	2.4	1.2	3.2	3.1	2.3
δ-OR (4N6H)	AT1R (4ZUD)	2.0	2.3	2.1	1.4	1.3	1.6	3.6	2.8	2.8
AT1R (4YAY)	CCR5 (4MBS)	2.7	2.3	2.1	1.9	1.6	1.4	2.5	2.4	2.4
M3R (4DAJ)	H1R (3RZE)	1.3	1.3	1.2	0.9	0.6	0.6	2.1	2.1	1.8
OX1R (4ZJ8)	DRD3 (3PBL)	2.8	2.3	2.3	2.0	1.6	1.6	3.9	3.5	3.5
FFAR1 (4PHU)	PAR1 (3VW7)	2.6	2.4	2.2	5.8	6.8	2.6	6.5	7.2	3.5
CRF1R (4K5Y)	GCGR (5EE7)	1.6	2.0	1.1	1.5	1.9	1.1	2.1	2.5	1.7
B2AR (2RH1)	B1AR (2VT4)	0.8	1.7	0.8	0.7	0.4	0.7	1.6	1.7	1.6
Average		2.0	1.9	1.7	2.0	1.8	1.5	3.1	2.9	2.5

Supplementary Table 3. Ligands docked to GPCRs in the binding specificity prediction benchmark. Columns 3-4: Measured dissociation constants of the ligand to two GPCR variants. Column 5: ddG: Measured ligand binding energy difference between the 2 GPCR variants. Column 6: ddG_predicted: Predicted ligand binding energy difference between the 2 GPCR variants in Rosetta Energy Unit (REU).

Ligand antagonists	Kd to D2 receptor (M)	Kd to D5 receptor (M)	ddG (Kcal/mol)	ddG_predicted (REU)
Haloperidol 	1.20E-09	1.00E-07	2.60	1.50
Spiperone 	8.00E-10	3.50E-06	4.90	3.20
S-Sulpiride 	1.50E-08	7.70E-05	5.00	2.61
BDBM50201338 	4.40E-08	3.90E-10	-2.75	-4.32
BDBM50306451 	9.30E-08	1.90E-09	-2.27	-2.55
Butaclamol 	9.40E-10	2.70E-09	1.96	0.81
BDBM50306327 	2.10E-06	7.00E-09	-3.32	-4.00

SCH23390		1.10E-06	3.00E-10	-4.60	-1.20
Ligand agonists		Kd to D2 receptor (M)	Kd to D2-S193G (M)	ddG (Kcal/mol)	ddG_predicted (REU)
Serotonin		1.36E-04	4.92E-06	-1.93	-2.09
Dopamine		3.45E-05	3.83E-04	1.4	1.7
Ligand antagonists		Kd to 5HT2B(M)	Kd to 5HT2A (M)	ddG (Kcal/mol)	ddG_predicted (REU)
Ketanserin		7.4E-07	8.1E-09	2.63	1.4
Volinanserin		1.0E-06	1.9E-09	3.65	0.2
Glemanserin		3.3E-06	2.6E-08	2.8	-2.05
RS-127445		1.1E-09	9.3E-07	-3.9	-2
SB-206553		2.2E-08	2.3E-06	-2.71	-0.8

SB-221284		2.5E-09	5.5E-07	-3.14	-2.87
LY 272015		7.5E-10	2.9E-08	-2.13	-2.06
Spiperone		1.10E-06	3.00E-10	4.79	3.7
Ligand agonist		Kd to 5HT1B (M)	Kd to 5HT1B-L126A (M)	ddG (Kcal/mol)	ddG_predicted (REU)
Ergotamine		4.79E-09	3.16E-09	0.242	0.02
Ligand agonists		Kd to 5HT1B (M)	Kd to 5HT1B-T134A (M)	ddG (Kcal/mol)	ddG_predicted (REU)
Ergotamine		4.79E-09	3.98E-09	1.07	0.22

Supplementary Table 4. GPCR targets for the ligand binding specificity benchmark. The sequence identity between target and template is reported for the entire aligned receptor sequence and for the ligand binding region which includes the extracellular half of the TM region and part of the extracellular loop 2 (Method). DRD2 active state models were used to predict the ligand agonist dopamine and serotonin binding specificity shifts upon mutations.

Target	Template	Sequence identity on full length(%)	Sequence identity on binding region(%)
DRD2	DRD3 (3PBL)	48.9	74.8
DRD5	DRD3 (3PBL)	30.5	37.7
5HT2A	5HT2B (4IB4)	56.0	54.9
5HT1B	DRD3 (3PBL)	37.4	35.6
5HT2B	DRD3 (3PBL)	33.0	30.0
DRD2 (Active)	B2AR (active state; 3P0G)	27.5	38.6

Supplementary Table 5. Designed dopamine D2 variants with altered ligand binding specificity. Upper table. Comparison between predicted and experimentally measured mutational effects on the binding energy of the 3 ligands. Predicted energies are provided in Rosetta Energy Unit (REU). Lower table. Measured mean pKd and standard error of the mean. All designed mutations had statistically significant effects on the binding of spiperone and SCH ($p < 0.05$, unpaired t-test) and no statistically significant effects on raclopride ($p > 0.05$, unpaired t-test).

Variants	Spiperone		SCH23390		Raclopride	
	Prediction (REU)	Experimental result (Kcal/mol)	Prediction (REU)/ Second round refinement (REU)	Experimental result (Kcal/mol)	Prediction (REU)	Experimental result (Kcal/mol)
WT						
V91M	1.28	0.68	-0.76	-0.62	0.09	0.16
V91W	2.80	1.83	-0.78	-1.01	0.18	0.05
V111L	2.10	0.37	-0.9/0.86	2.80	-0.04	-0.11
V111I	2.30	0.80	-1.1/0.23	1.40	-0.12	0.04
C118I	-0.22	N.D.	-0.40	N.D.	N.D.	N.D.
T412L	-0.17	-0.40	-0.55	-1.53	0.21	0.47
V91W, T412L	3.20	2.12	-1.03	-2.17	0.17	0.06

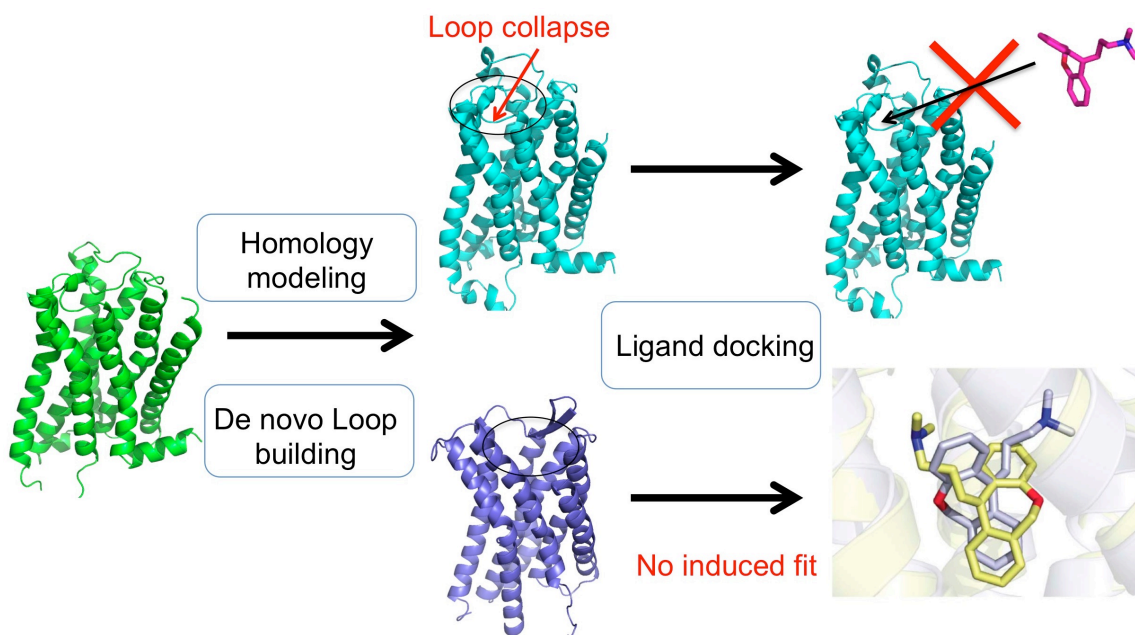
mean pKd and SEM									
Variants	Spiperone			SCH23390			Raclopride		
	pKd	SEM	number of repeats	pKd	SEM	number of repeats	pKd	SEM	number of repeats
WT	8.9	0.06	3	5.9	0.09	6	8.5	0.09	3
V91M	8.4	0.03	3	6.4	0.12	6	8.4	0.1	3
V91W	7.5	0.07	3	6.7	0.08	4	8.5	0.09	3
V111L	8.6	0.05	3	3.8	0.10	4	8.5	0.08	3
V111I	8.3	0.05	3	4.8	0.50	4	8.5	0.06	3
C118I	N.D.	N.D.	N.D.	N.D.	N.D.	N.D.	N.D.	N.D.	N.D.
T412L	9.2	0.07	3	7.0	0.19	4	8.2	0.12	3
V91W, T412L	7.3	0.4	4	7.5	0.50	4	8.5	0.15	3

Supplementary Table 6. Structural diversity of the ligand-bound dopamine D2 receptors. Structural comparison between the homolog template D3 receptor and the selected models of distinct ligand-bound D2 receptors over the ligand binding region.

Binding region C α RMSD / binding region all atom RMSD (Å)			
	D2-SCH23390	D2-Spiperone	D2-Raclopride
D3 (3PBL)	0.67/-	0.65/-	0.66/-
D2-SCH23390		0.48/0.97	0.64/1.37
D2-Spiperone			0.61/1.32

Supplementary Figures

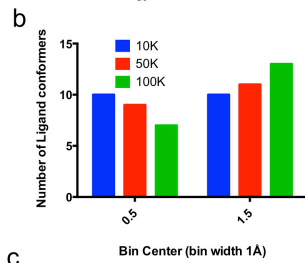
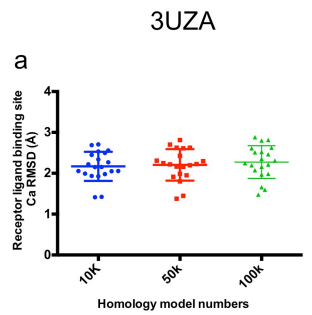
Supplementary Figure 1. Inherent flaws of sequential modeling/docking approaches. Ligand-free receptor structures are modeled by first *de novo* reconstructing poorly aligned regions and then relaxing the entire rebuilt structure. A fraction of the models will undergo “loop collapse” partially occluding the ligand binding site and preventing the ligand to find its native bound conformation. In traditional ligand docking simulations, the receptor structure is not fully relaxed, preventing the modeling of induced fit effects upon ligand binding.



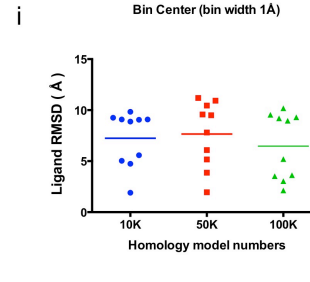
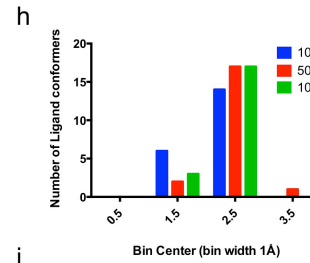
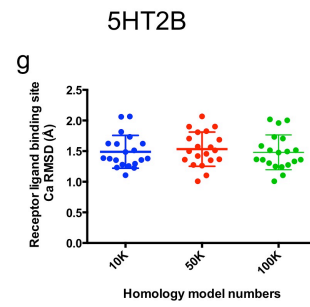
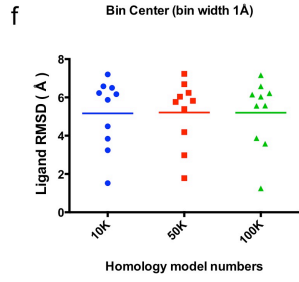
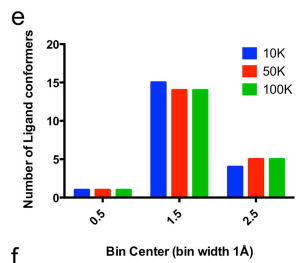
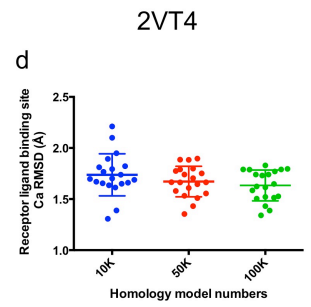
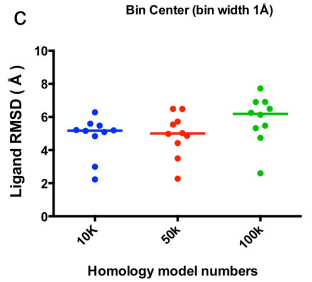
Supplementary Figure 2. Effect of the number of trajectories on the sampling of ligand and receptor conformational diversity and on the prediction accuracy.

Conformational diversity and structural accuracy of models selected from 10000 (blue), 50000 (red) and 100000 (green) independent trajectories for 3 selected GPCR targets, 3UZA, 2VT4 and 5HT2B. **a, d, g.** Distribution of ligand binding site Ca rmsd to the native structure of 20 selected receptor models. These models correspond to the center receptor structures of the 20 largest families of 10% lowest energy ligand-bound receptor models after all-atom relaxation (step3, Method). **b, e, h.** Distribution of the ligand conformational diversity (measured by heavy atom rmsd) for the ligand poses bound to the 20 receptor models selected after all-atom relaxation (step3, Method). The ligand heavy atom rmsd is calculated after alignment of the ligand model conformation to the native ligand conformation. **c, f, i.** Accuracy of the ligand bound conformations (measured by heavy atom rmsd to the native structure) for the 10 selected ligand-bound receptor models after ligand docking refinement (step4, Method). The ligand heavy atom rmsd is calculated after alignment of the model and native receptor structures. These results support our selection of 10000 trajectories which represent an appropriate tradeoff between efficiency and accuracy.

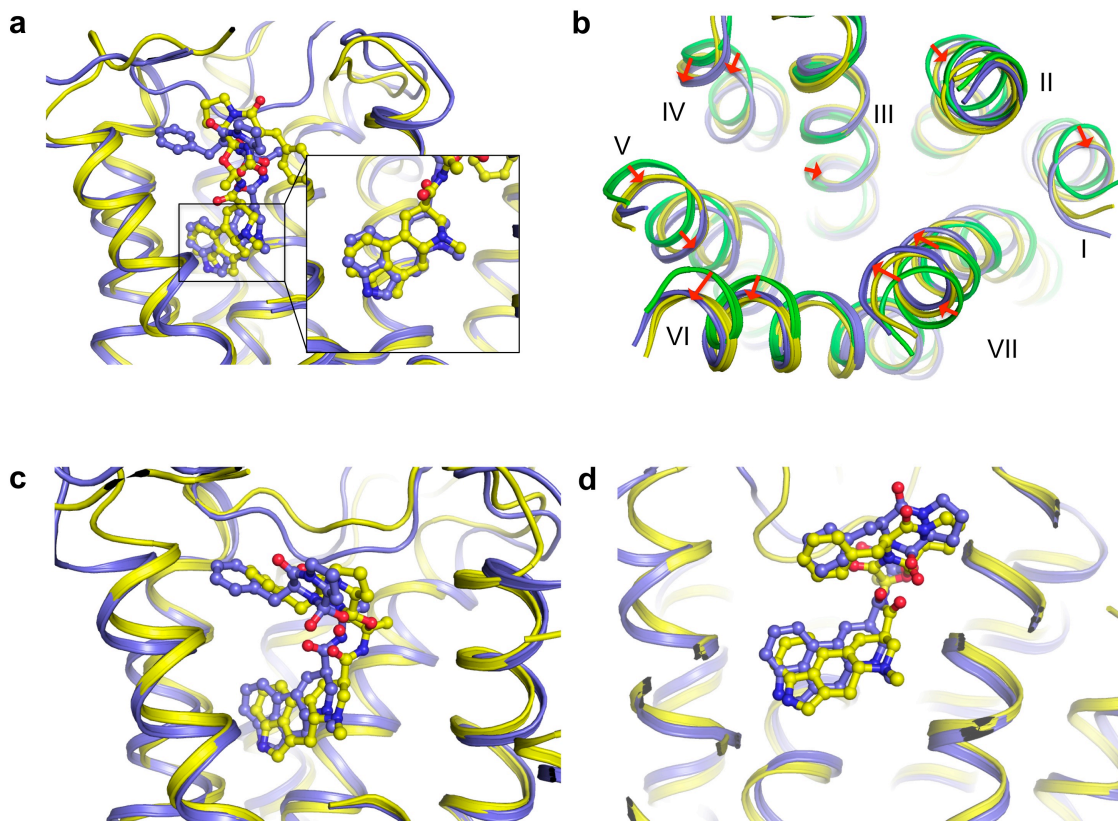
Steps 1-3: loop rebuilding with bound ligand and ligand-bound receptor relaxation



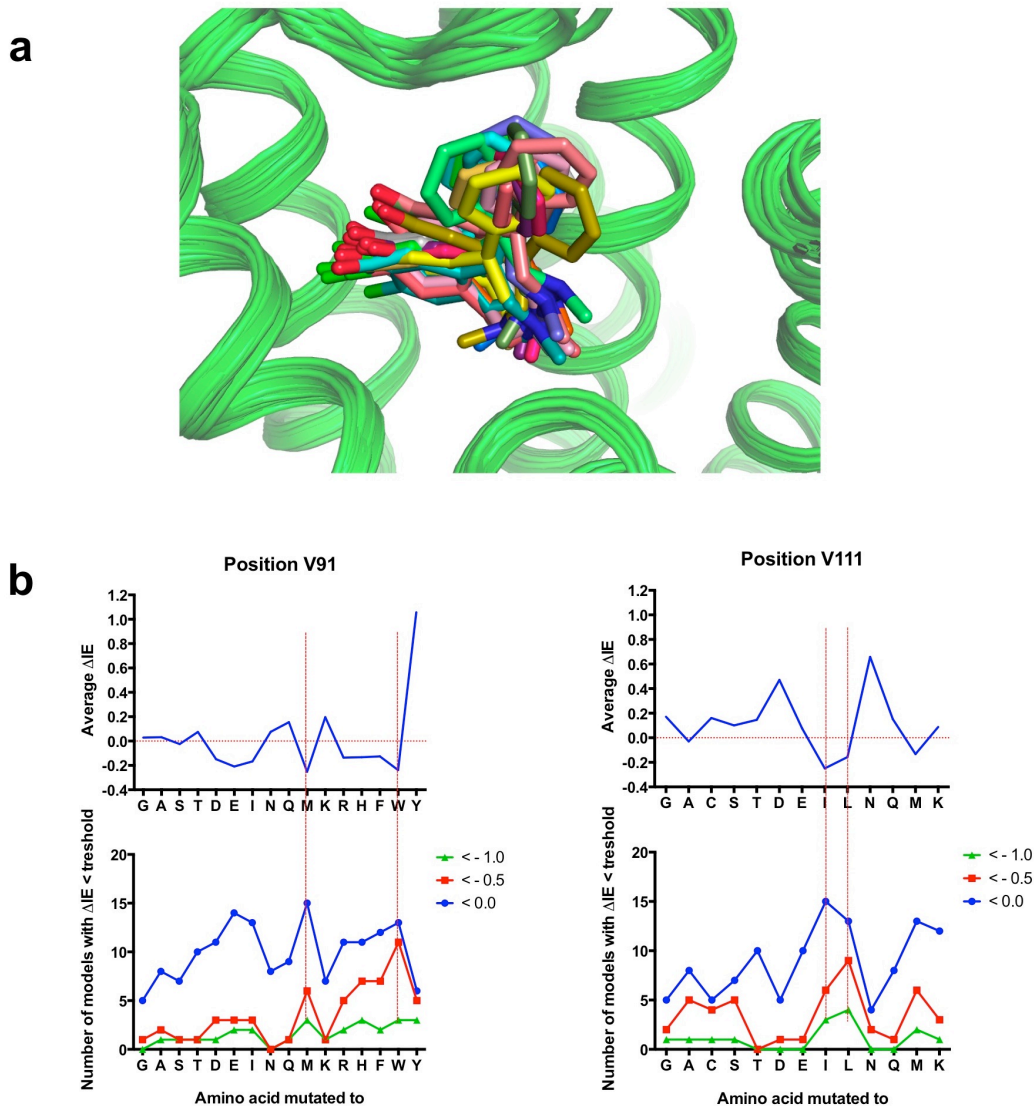
Step 4: ligand docking refinement



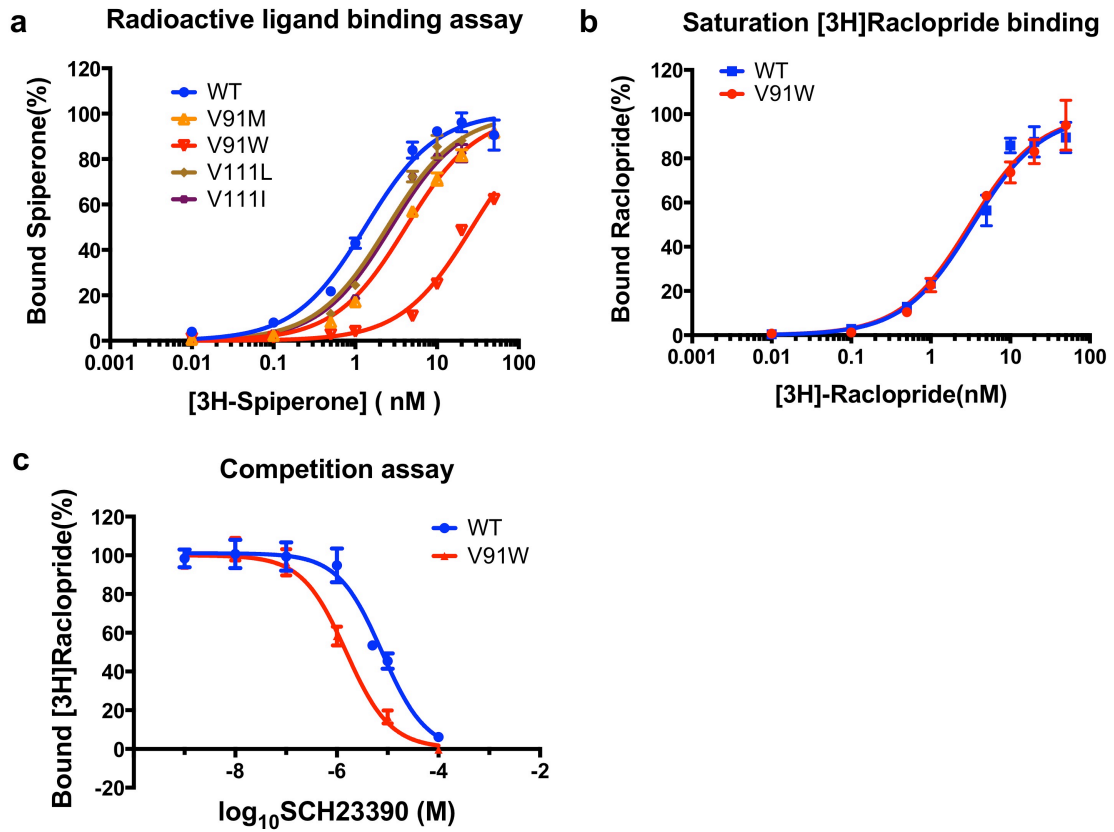
Supplementary Figure 3. Blind (GPCR-DOCK 2013) and benchmark predictions of ergotamine-bound serotonin receptor structures. **a.** Blind predicted model ranked #1 of 5HT2B (yellow) superimposed onto the 5HT2B X-ray structure (blue). The ergotamine core of the ergotamine ligand (zoom caption) has a heavy atom rmsd of 0.97 Å to the native while the full-length ergotamine ligand rmsd is 4.7 Å. **b.** Detailed improvement of the 5HT2B ligand binding site structure. Blind predicted model ranked #1 (yellow) of 5HT2B superimposed onto the 5HT2B X-ray structure (blue) and onto the starting dopamine D3 template structure (green). Red arrows indicate substantial improvements toward the target structure. Transmembrane helix number is indicated. **c, d.** Benchmark models of ergotamine bound 5HT2B (**c**) and 5HT1B (**d**). The full-length ergotamine ligand rmsd is 1.9 Å (**c**) and 1.4 Å (**d**). Models (yellow) superimposed onto the Xray structures (blue).



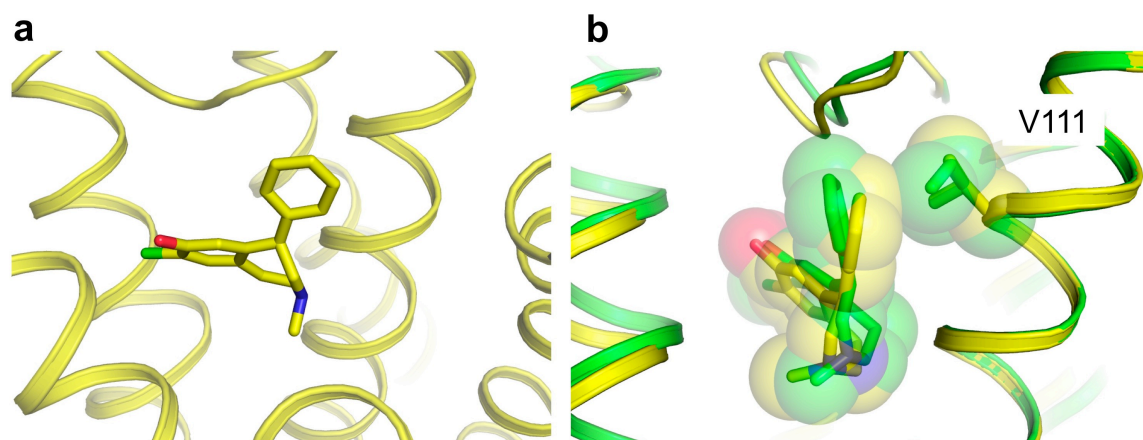
Supplementary Figure 4. Design of mutations displaying consensus effects on ensembles of receptor-ligand conformations. **a.** Superposition of 20 representative low energy SCH23390-bound D2 receptor models. **b.** Predicted effects of designed amino-acid substitutions on the 20 models given by the average energetic effect (upper panel) and by the number of models with predicted energy difference from WT (ΔIE : difference in ligand-receptor interface energy in Rosetta Energy Unit) for 3 distinct ΔIE thresholds (lower panel). Amino acids displaying the largest consensus effects are selected for experimental validation (red dotted lines).



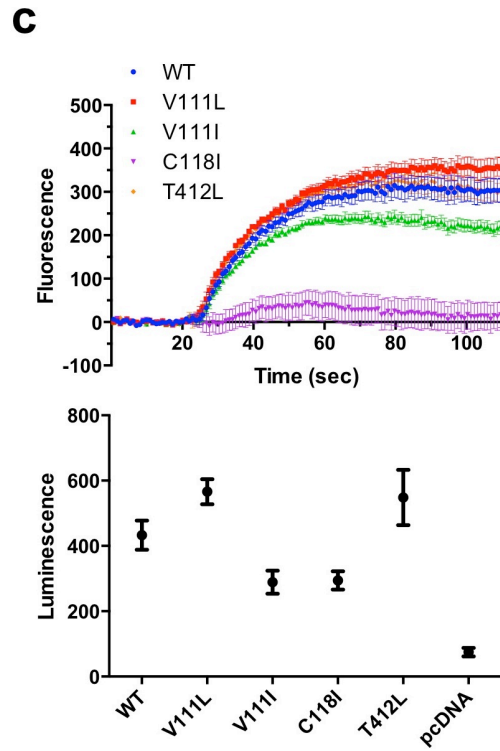
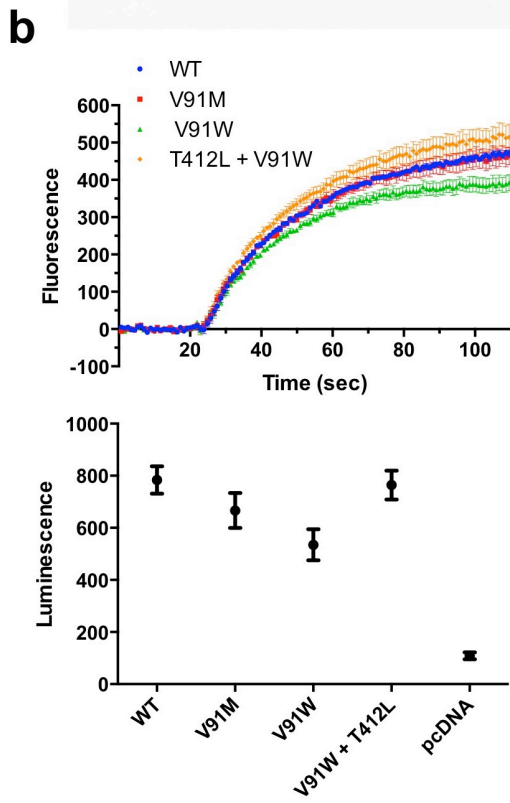
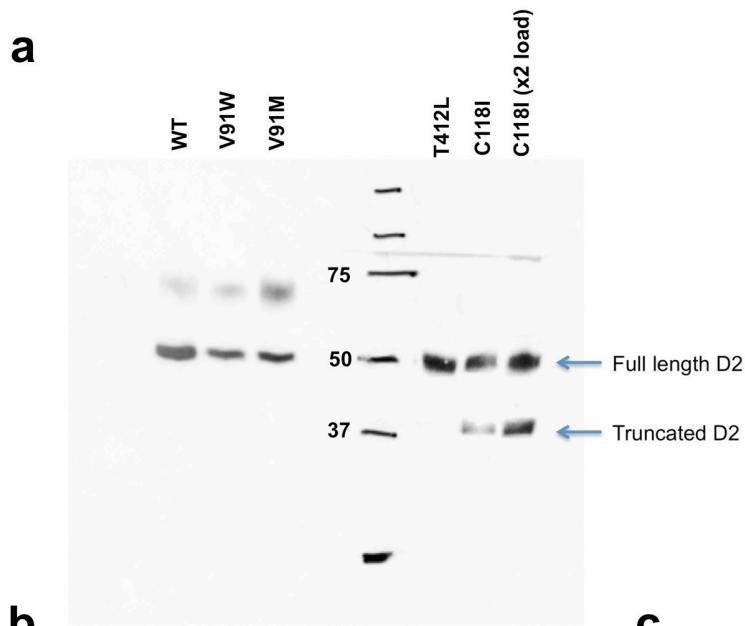
Supplementary Figure 5. Radioligand binding to dopamine D2 receptor. a-c. Ligand binding curves measured for designed D2 receptor variants titrated with Spiperone (a), Raclopride (b), SCH23390 (c).



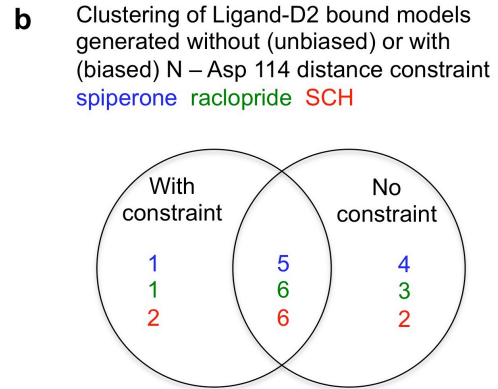
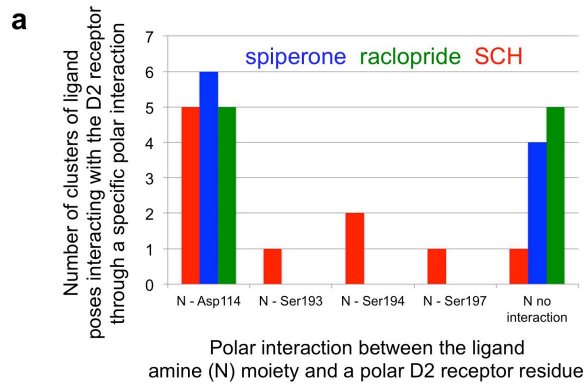
Supplementary Figure 6. Experimentally-guided refinement of SCH23390-bound D2 models. **a.** The binding mode of the final selected SCH23390-bound D2 models after experimental refinement. **b.** Detailed comparison of the SCH23390 conformation between the final selected model (yellow) and one of the models selected for the first round of design calculations (green). The interface energy and ligand conformations are very similar (interface energy difference = 0.6 Rosetta Energy Unit, Lrmsd = 0.9Å) between the two models. However, the ligand pose selected for the first round of design calculation was predicted to be stabilized by the V111I mutation (as shown by good shape complementarity) while the final selected model displays a steric clash with the isoleucine mutation corroborating the experimentally measured loss in binding affinity.



Supplementary Figure 7. Designed D2 variants respond to dopamine and activate Gi. **a.** Western blots of membrane fractions of HEK293T cells transiently expressing D2 designed variants used for radioligand binding assays (two blots performed in distinct experiments were concatenated and are separated by the marker lane). WT, V91M, V91W and T412L variants are shown as examples to comparison with C118I. Unlike the other variants, C118I displays two bands: one with a MW corresponding to the full length receptor; one with a MW corresponding to an N-terminal fragment of a cleaved version of the receptor. Our observations suggest that C118I destabilizes the receptor which cannot adopt the proper structure for binding and responding to any extracellular ligand. Additionally, this instability leads to partial degradation and cleavage of the receptor. Note: the faint band at MW=70kD is not observed consistently in our sample preparation. Ligand binding results are not affected by the presence of this band. **b,c.** Upper panels. TrpC4beta channel activation by Gi upon dopamine induction (at time t = 20 sec) measured by change in fluorescence of a probe reacting to cation intracellular flux (Method). Cells stably expressing Trp channels were transfected with plasmids expressing designed D2 variants. All fluorescence traces reported for the D2 variants were subtracted from signals measured for Mock samples (cells transfected with empty pcdna vectors) under identical conditions. Lower panels. Cell surface expression of D2 variants measured by Elisa (Method).



Supplementary Figure 8. Blind unbiased docking of the ligands on D2 receptor generates models recapitulating designed mutational effects. a-b. Data for the 3 ligands are represented (spiperone: blue; raclopride: green; SCH: red). **a.** Number of clusters of low energy ligand-D2 bound poses displaying a specific polar interaction between the ligand amine (N) moiety and a receptor residue. **b.** Venn diagram of the distribution of ligand-D2 bound poses generated with or without N-Asp 114 constraint in 10 clusters of different structures. When clustered together (cluster rmsd threshold = 2.5 Å), a majority of ligand bound D2 poses generated with or without constraint gather in the same families of structures (more clusters and models belong to the cross section of the 2 circles). Therefore, these models have very similar conformation. This analysis is performed separately for the three distinct ligands bound to D2 (spiperone: blue; raclopride: green; SCH: red). **c.** Designed mutations often display the desired and experimentally validated effects on the binding energy of the 3 ligands when calculated using the “unbiased” ligand-bound D2 structures from the most converged simulations (i.e. displaying the consensus polar interaction with the receptor). For each ligand, ligand – bound D2 models are gathered in 3 categories of energetic effects on ligand binding affinity (Method): decreased affinity (green), increased affinity (blue), minor change in affinity (red). According to these design calculations, V91W, V91M, and V111L display the intended predicted effects on the 3 ligands and would have been selected for experimental validations. *: blind predicted effect matches the experimental observation.



c Predicted designed mutational effect on ligand binding calculated using unbiased ligand-D2 bound models displaying the consensus N – Asp 114 polar interaction

